Intense Raman D band without disorder in flattened carbon nanotubes

Emmanuel Picheau, Anthony Impellizzeri, Dmitry V. Rybkovskiy, Maxime Bayle, Jean Yves Mevellec, Ferdinand Hof, Hassan Saadaoui, Laure Noé, Abraao Cefas Torres Dias, Jean-Luc Devail, et al.

'Intense Raman D Band without Disorder in Flattened Carbon Nanotubes'

E. Picheau, A. Impellizzeri, D. Rybkovskiy, M. Bayle, J.-Y.Mevellec, F. Hof, H. Saadaoui, L. Noé, A. Dias Torres, J.-L. Duvail, M. Monthioux, B. Humbert, P. Puech, C. P. Ewels, A. Pénicaud

ACS Nano, 15 (1), 596-603 (2021)

Intense Raman D Band without Disorder in Flattened Carbon Nanotubes

*Emmanuel Picheau,[1] Anthony Impellizzeri,[2] Dmitry Rybkovskiy,[3] Maxime Bayle,[2] Jean-Yves Mevellec,[2] Ferdinand Hof,[1] Hassan Saadaoui,[1] Laure Noé,[4] Abraao Cefas Torres Dias,[4] Jean-Luc Duvail,[2] Marc Monthioux,[4] Bernard Humbert,[2] Pascal Puech,[4] Christopher P. Ewels,[2] Alain Pénicaud[1]**

[1]Université de Bordeaux, CNRS, Centre de Recherche Paul Pascal, UMR5031, 33600 Pessac, France.

[2]Université de Nantes, CNRS, Institut des Matériaux Jean Rouxel, IMN, F-44000 Nantes, France.

[3]Skolkovo Institute of Science and Technology, Skolkovo Innovation Center, 121025, 3 Nobel Street, Moscow, Russia.

[4]CEMES, UPR8011-CNRS, Université de Toulouse, 29 rue Jeanne Marvig, 31055 Toulouse CEDEX 04, France.

ABSTRACT:

Above a critical diameter, single or few-walled carbon nanotubes spontaneously collapse as flattened carbon nanotubes. Raman spectra of isolated flattened and cylindrical carbon nanotubes have been recorded. The collapsing provokes an intense and narrow D band, despite the absence of any lattice disorder. The curvature change near the edge cavities generates a change of hybridization that activates a D band, despite framework continuity. Theoretical calculations based on Placzek approximation fully corroborate this experimental finding. Usually used as a tool to quantify defect density in graphenic structures, the D band cannot be used as such in the presence of graphene fold. This conclusion should serve as a basis to revisit materials comprising structural distortion where poor carbon organization was concluded on Raman basis. Our finding also emphasizes cultural differences in understanding of a defect between chemists and physicists, a source of confusion for researchers working in nanotechnologies.

TOC FIGURE

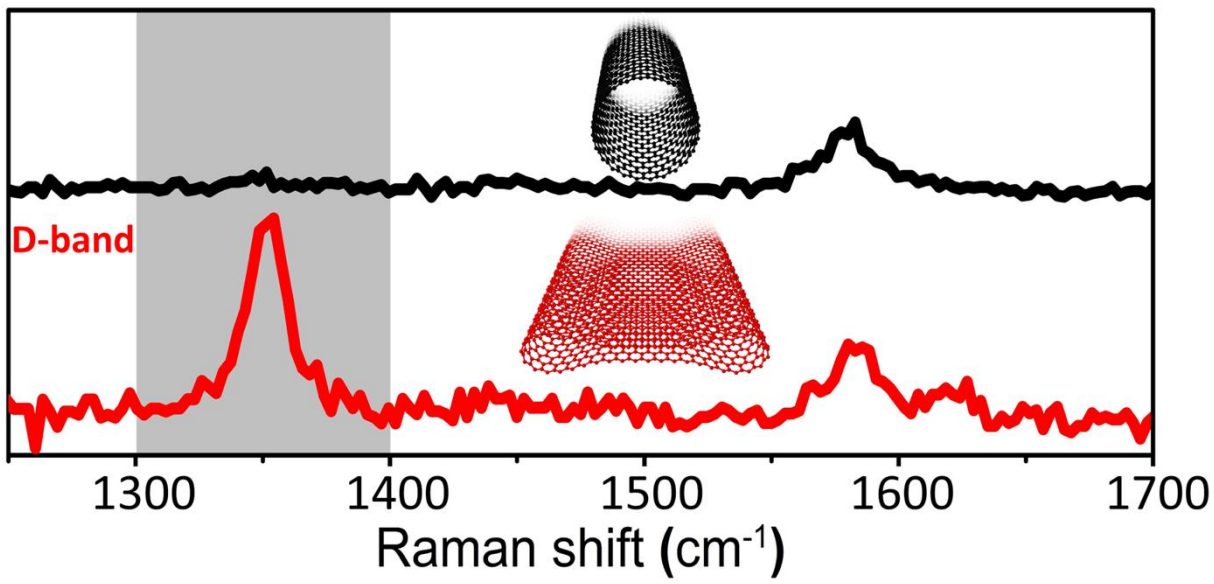

TOC comment: Flattening provokes an intense and narrow Raman D band in carbon nanotubes.

Keywords: Raman spectroscopy – Collapsed carbon nanotubes – Defects – Raman D band - Carbon nanotubes – Flattened carbon nanotubes

Raman spectroscopy is a sensitive technique particularly well adapted to characterise carbon nanomaterials.[1–12] Notably, the so-called D band has been studied and used extensively to characterise lattice defects in carbon materials, both qualitatively and quantitatively.[13–15] However, a D band does not always account for topological defects and can easily be misinterpreted.[8] Furthermore different visions of what a defect is between physicists (any translational symmetry breaking) and chemists (topological view) can confuse researchers working with nanomaterials. Unambiguous attribution of a D band is thus of primary importance for generalization in the broad family of nanocarbons. Flattened carbon nanotubes (FCNTs, scheme in Fig. 1d) can be considered as few-layer graphene nanoribbons (GNRs) with continuity at the edges.[16–20] They overcome the as-yet unsolved difficulty to obtain scalable GNRs with atomically-smooth edges, critical for electronics.[21] To date there are very few reported Raman spectra of self-collapsed FCNTs,[22,23] and in these studies the objects were not identified as FCNTs but as GNRs. We report here the Raman signature of clearly identified, individual self-collapsed FCNTs, together with quantum chemical Raman spectra simulations of these large objects. Strikingly, the collapse provokes the appearance of an intense and narrow D band, independent of the presence of topological defects. Therefore, flattened carbon nanotube can be used as an ideal object to determine Raman cross section of the D band over the G band. This unusual origin for a D band, which arises solely as a signature of folding, should have wide repercussions for the field of graphene and related materials regarding defect quantification, as well as in theory, since it can be used to calibrate the relative D band intensity as a function of that of the G band.

RESULTS AND DISCUSSION

FCNTs were obtained by extracting nested tubes from multi wall carbon nanotubes (MWCNTs). After opening their caps by thermal oxidation, MWCNTs were sonicated in solution (see fig.S1 in ESI, experimental section). This previously reported process removes inner tubes from the MWCNTs,[24] leaving large single- or few-walled nanotubes which are no longer stable and self-collapse into FCNTs driven by interlayer attractive interaction. Single wall carbon nanotubes spontaneously self-collapse for diameters above 5.1 nm.[25,26] The resultant solution contains both MWCNTs (blue arrows Fig. 1a) and FCNTs (orange arrows Fig. 1a) as shown in the TEM image. Most MWCNTs exhibit inner cavity diameters below 3.5 nm and several graphene layers (8 to 30 tubes), typical of the parent MWCNTs. These tubes are either not opened or have only undergone partial extraction. In contrast, FCNTs possess large width (>5nm) and very few graphene layers. Such objects are not observed in the untreated MWCNT sample. Notably one object (red arrow Fig. 1a) has both a non-collapsed (right) and collapsed part (left). The external diameters for both sides ($\approx$ 5 nm and $\approx$ 7 nm) are consistent with collapsing (width $\approx \pi$ x diameter /2, inset Fig. 1a) rather than an unzipping process (width = π x diameter), initially proposed by Jiao et. al.[22] and later contested by Choi (see also ESI Theoretical section and Fig.S16).[24] The transversal scheme of a FCNT in Fig. 1d shows they consist of two longitudinal cavities, linked by a central flat region composed of multi-layer graphene. These two cavities in the atomic force microscopy (AFM) height profile Fig. 1d unambiguously confirm the flattened character of the object shown in AFM height (Fig. 1b) and phase (Fig. 1c) imaging. The cavities are also visible as contrast in the AFM images. We attribute the phase contrast to the change of local strain imposed by the longitudinal cavities and the concomitant rolling of the graphene sheet onto itself. The asymmetric cross-section with raised edge cavities is also visible with scanning electron microscopy (SEM, Fig. 1e and S9, ESI).

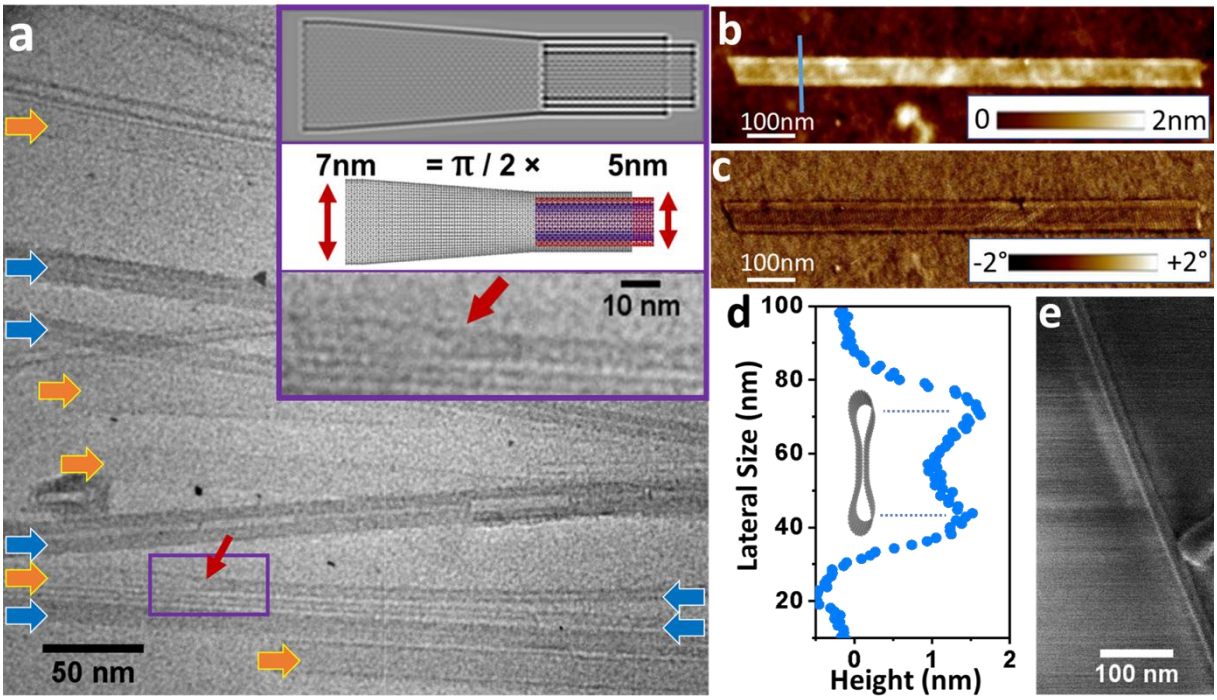

Figure 1 a) TEM image showing MWCNTs (blue arrows) and FCNTs (orange arrows). The inset shows the collapse from a MWCNT (right) to a FCNT (left), indicated by a red arrow (middle image is an AIREBO potential optimized atomic structure, top the corresponding TEM simulation). b,c) AFM image of a FCNT deposited on a substrate (silicon wafer with 300 nm SiO2 layer) in (b) height and (c) phase. d) AFM Height profile along blue line in b and scheme of a FCNT. e) SEM image of a FCNT on a silicon wafer (primary electrons 1 kV acceleration voltage, no conductive coating, see also ESI and Fig. S9)

Figure 2a shows an AFM image in the vicinity of the FCNT shown in Fig 1b-c, revealing five additional elongated objects. By carefully superposing a spatial map of Raman G-peak intensity onto this AFM image, each object can be unambiguously assigned a Raman spectrum (see ESI Fig. S2 to S5). Fig. 2b shows the corresponding Raman spectra. Three MWCNTs and two further FCNTs were identified. It is possible to attribute the flattened (FCNT) or cylindrical (CNT) character of each object from their height in the topological AFM image. These values are based on the mean of 6 self-consistent line profiles for each

object. The two species are clearly distinct: FCNTs 1, 2 and 3 have heights below 3 nm, whereas CNTs 1, 2 and 3 have heights above 5.8 nm (see inset in Fig2a).

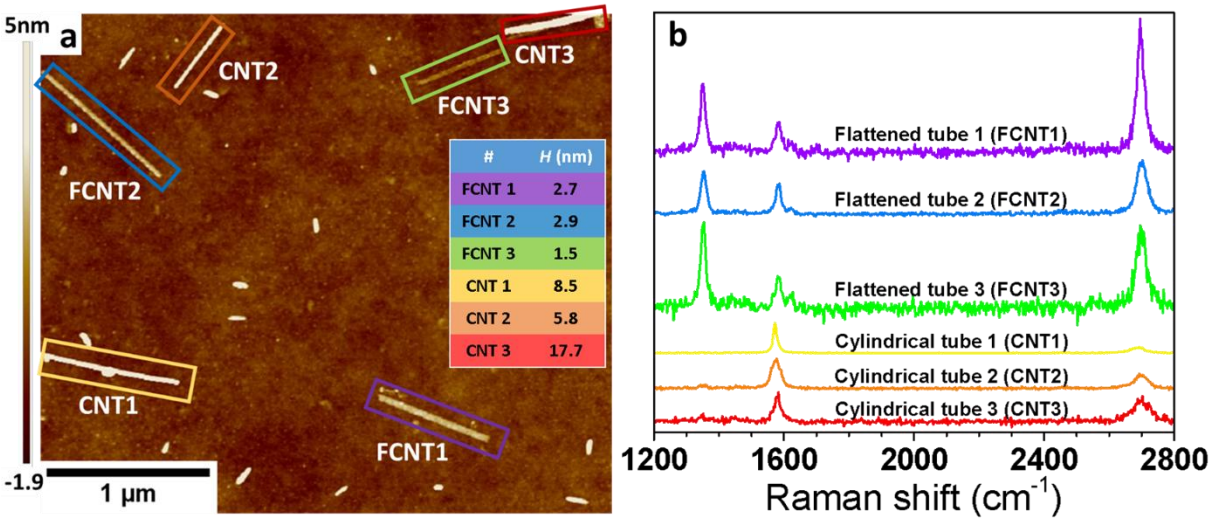

Figure 2 a) AFM height image of 3 flattened (FCNT) and 3 cylindrical (CNT) nanotubes. Inset: their respective height H (nm). All values are obtained from the same image, i.e. recorded with a single tip. b) Corresponding Raman spectra normalized over the G peak (around 1580 cm^{-1}), recorded at 514 nm (2.41 eV) with incident polarisation parallel to the principal axis of FCNT1.

From this attribution, Figure 2b allows direct comparison of the Raman signal for CNTs and FCNTs. The spectra are composed of G (≈ 1580 cm^{-1}) and 2D (≈ 2700 cm^{-1}) peaks, typical of *sp*2 carbon[2] and D (≈ 1350 cm^{-1}) and D' (≈ 1620 cm^{-1}) peaks, commonly attributed to structural defects.[2,13] The attribution as a D band to the peak at ~1350 cm^{-1} for FCNTs is based on its highly dispersive character (see ESI, Fig.S11 in D band dispersion section); ~60 eV/cm^{-1} is typical for double resonance processes in other graphitic materials.[27] The Raman spectrum of the parent MWCNT powder taken at 532 nm (2.33 eV, Fig. S8) closely resembles the spectra of CNT1 to CNT3. The spectra of FCNTs and CNTs are strikingly different; of particular note is the presence of a strong D peak in the case of FCNTs, absent or quasi-absent for CNTs (Fig. 2b). A second difference is the presence for FCNTs and absence for CNTs of a D' band. Finally, FCNTs show a 2D band typical of few uncorrelated graphene layers

(intense, narrow with FWHM below 36 cm^{-1}, and of single Lorentzian shape), whereas for CNTs the 2D band has much lower relative intensity, and is broader (FWHM above 45 cm^{-1}, see fits in ESI Fig.S10 and Table S1) with a complex shape. The FWHM and A(2D)/A(G) are given in Table S2. Finally, contrary to CNTs and as expected,[28] FCNTs do not show any antenna effect, i.e. the global Raman intensity is not influenced by the relative orientation between the object axis and the light polarization (see the depolarization effect in ESI, Fig. S12 to S15 in polarization dependency measurement section and Fig. S6).

To activate a D (and D') band, the excited electron should be elastically backscattered by an inhomogeneity in the electronic potential.[2,11] Since local structural and chemical defects necessarily break the symmetry, the D/G peak relative intensity is commonly used to estimate defect types and density, hence the degree of functionalization of a carbon material.[2,13–15] For GNRs especially, D band intensity has been used as a basis to discuss edge quality and orientation (armchair/zig-zag).[2,10,11,23,29,30] Our CNTs and FCNTs come from exactly the same solution, having undergone identical physical and chemical treatments, and so their defect density is expected to be similar. Since the MWCNTs exhibit no D band, this means that the sharp and intense FCNT D band is not due to local structural defects. Instead, we assign it to the presence of lateral edge cavities, as demonstrated below.

Incident polarisation dependency measurements (see Fig. 3a and ESI) show that the D band intensity is highest when the light polarization is parallel to the cavities and minimal when the polarization is orthogonal. This peanut shape dependency on polarisation (Fig. 3a, S13c & S14c) is fully consistent with a D band originating from a iTO phonon, activated by the cavities parallel to the tube axis. In fact, when the light polarisation and the cavities are parallel, the iTO phonon allows the electron to travel orthogonally to the cavity. The electron then arrives with a normal incidence compared to the cavity allowing backscattering. On the

contrary, when the light polarization is orthogonal to the cavity the electron is scattered (by the phonon) in a direction parallel to the cavity and may never reach it.

This model is further supported by the narrow bandwidths seen for FCNTs (≈ 18 cm^{-1}, Table S2), which demonstrates there are only few, randomly distributed defects, i.e. the electronic band structure is preserved. Edge curvature does not create electronic levels nor charge localisation around the Fermi level.[19] Instead the electron (or hole) is scattered by an iTO phonon and backscattered by the localised curvature before photon emission by electron-hole recombination. There are multiple scattering mechanisms possible associated with the edge of a collapsed nanotube. These include (i) direction change of the electron wave packet, as it moves around the curved edge from the top to bottom dogbone surface, resulting in an inversion of the k-vector and a switch of associated k-space valley, (ii) local change in curvature at the interface between the flat central region and the start of the edge. This involves a small out-of-plane rehybridisation of the carbon atoms, which can act as an electrostatic potential scattering barrier (Figure 3b-d), (iii) the change from bilayer to two fully decoupled separated layers as the folded edge is approached breaks the symmetry and acts as a scattering barrier, particularly in the situation where the electron wave packet in the central region is distributed across both top and bottom layers. In practise all these mechanisms may be acting in parallel and it is difficult to distinguish between them. They are all manifestations of the same underlying structural change, namely *localisation of curvature* at the edge of the collapsed carbon nanotube. The D-band peak is narrow (full width half maximum of only ~18 cm^{-1}) compared to a more conventional defect-driven D-band. This is both because of the lack of disorder in the sample (as demonstrated by the absence of D-band in the cylindrical tubes in the sample), and in particular, because the folded edge structure is highly uniform with no roughness along the length of the FCNT. Among the ten thousand or more Raman articles on carbon materials, to the best of our knowledge, there is only one

phenomenological report of a D band related to folding, and that without physical interpretation.[31] That experimental evidence actually confirms our finding. This work thus appears as an extension of graphene edges. However, in FCNTs, there is no *a priori* limit, the graphene sheet being continuous everywhere, contrary to graphene edges where the termination of the structure is a physical limit to any propagation.

The central zone of a FCNT is a twisted bi-layer, which could be associated to phonon activation and needs to be considered in addition to the activation associated with the two edge cavities. In the case of twisted graphene bi-layers, additional features are visible, due to intralayer and interlayer electron–phonon interactions.[12] However, as the signal for FCNTS never presents features associated to intralayer and interlayer electron–phonon interactions, neither here nor in a previous report where they were erroneously identified as GNRs[22](vide infra) we believe that the lateral size of FCNTS is not large enough to give an observable Raman signal contrary to twisted bi-layer graphenes. Furthermore, as the D band observed for FCNTs is dispersive and no other band is observed, the Raman spectrum is dominated by both the classical G band and the D band activated by the localisation of the curvature at the edge.

While an isolated CNT has a homogeneous electronic potential, and thus no elastic backscattering is possible, in FCNTs the situation is different. Figure 3 shows the density functional theory (DFT) optimised curvature of a FCNT, free-standing (c) and interacting with a surface (d). Tube curvature is pronounced at the edge (black arrows) and between the flat zones (red arrows), where the atomic orbitals distort causing partial sp2-sp3 rehybridisation.[32] The associated change in electronic potential corresponds to a barrier which is associated with a reflection coefficient. Thus, the electron (or hole) can be elastically backscattered, inducing a structural defect-free D band. Conservation rules must be respected which implies that the D band is activated for an armchair fold (zig-zag tube) and not for a

zigzag fold (armchair tube, vide infra). The same occurs with GNRs where the edge structure determines the presence or not of a D band.[10]

We can now estimate the C_a factor, which represents the effect on I_D/I_G, of the area able to activate a D band at the periphery of a point defect, but without being part of the structurally disordered zone. When considering only the peripheric area, Ca is defined as the proportionality factor linking I_D/I_G with the total fraction of this area. [15] To evaluate the fraction of the object able to activate a D band, a width W of *ca* 30 nm for FCNT1 is considered (see AFM profile Fig.1d) and an activation of the D band up to $r_a = 3$ nm on each side of the line of curvature change (value from ref.[15]). Thus, we have $I_D/I_G = C_a*(4r_a/W)$, i.e. $C_a \approx 5.5$. for FCNT1 ($I_D/I_G = 2.2$), giving an estimate for the three FCNTs (Ca~9 for FCNT3, probably due to quasi-zigzag (optimal) nanotube). These values are larger than the value obtained for a point defect (4.2 in ref.[15]) showing that the whole intensity for the D band measured for FCNTs is explained by the two lateral cavities generating a zone that activates a D band, and is exempt of any structural disorder. This definitely validates the interpretation of the D band as activated by localization of curvature at the edge.. A more sophisticated analysis[13] shows that a line defect approach leads to a lower D-band intensity, proving that D-band activation in FCNTs is beyond all known systems. Thus, FCNT are perfect candidates to measure the C_a factor, a key parameter in the field, to merge calculations mixing third and fourth order of the perturbation theory approaches.

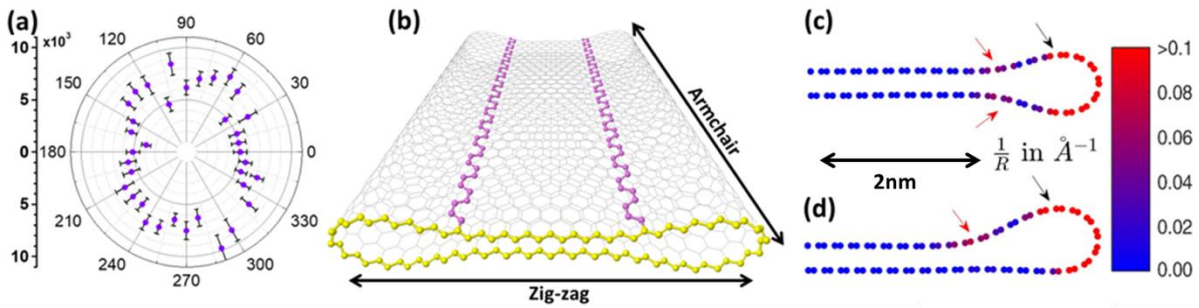

Figure 3 a) D band intensity vs incident polarization for FCNT1 (no analyzer was used for the scattered light), normalized by the experimental TO peak area of the silicon substrate (100)

and compensated for the theoretical polarization dependence of the TO peak area of the silicon substrate, to account for the different polarization dependency of the substrate and the objects (see ESI). The incident light polarization was kept fixed along the 90°-270° axis while the object was rotated of an angle θ (details in ESI). Thus the angle θ=0 correspond to a situation where FCNT1 was orthogonal to the light polarization and θ=90 correspond to a situation where FCNT1 was parallel to the light polarization. A similar dependency has been obtained for FCNT2 (Fig. S14). b) Schematic of a zig-zag FCNT showing the armchair line of hybridization change. Curvature of a FCNT c) Free standing, d) On a substrate. The color scales according to the local curvature.

Nanocarbon Raman spectra are commonly simulated using perturbation theory, which allows for an accurate description of resonant scattering processes.[33] This method, however, requires the evaluation of electron-phonon matrix elements over the entire Brillouin zone, which is computationally too demanding for large systems with hundreds of atoms, as is the case for FCNTs. Here we use the Placzek approximation instead, based on the evaluation of the dielectric function derivative with respect to phonon eigendisplacements. The method has successfully described the Raman spectra of narrow graphene nanoribbons.[34,35] DFT calculations are used to obtain phonon frequencies and eigenvectors at the gamma point of the one-dimensional Brillouin zone of the FCNT. We then displaced the equilibrium geometry of the FCNT along the eigenvectors of each phonon mode and evaluated the corresponding frequency-dependent dielectric function. The derivatives of the dielectric function with respect to the eigendisplacements were then used to obtain the Raman tensors for different excitation wavelengths (details in ESI Computational method section). The resulting spectra were obtained by averaging the polarizations of incident and scattered light in the plane of the FCNTs and applying a Lorentzian broadening of the peaks. The method successfully predicts

D band free spectra for cylindrical SWCNTs, as well as the appearance of a broad D band upon introduction of a point defect (ESI Theoretical section and Fig.S17).

We recall that CNT type (zig-zag, armchair, chiral) refers to the arrangement of carbon atoms around the tube circumference, while GNR notation refers instead to the atom arrangement along their length. For FCNTs, we follow the nanotube notation and hence, for example, a (70,0) zig-zag FCNT has carbon atoms in zigzag orientation around its circumference and armchair orientation along its length (Fig 3b). Tangential shear allows the interlayer stacking of a collapsed tube to vary. In our calculations, the lowest energy interlayer stacking was considered (AB' for the (70,0)), although interlayer stacking was varied (see Fig. S17) and does not qualitatively change the results and conclusions.

The calculated Raman spectrum for a flattened (70,0) nanotube at 2.3 eV excitation energy (538 nm) is shown in Figure 4, with eigendisplacements associated with key peaks below it. The spectrum shows two main peaks at 1371 and 1564 cm^{-1}. The eigendisplacement corresponding to the 1371 cm^{-1} peak exhibits "breathing" of individual hexagons, resembling the phonon shape common for the graphene-iTO branch near the K-point of the hexagonal Brillouin zone. These phonons are known to participate in the defect-induced D band of graphene.[36] Note that the same calculation on the same, unflattened, 70,0 tube shows no D band (Fig 4, top). The cavities break the lattice symmetry as described above and couple these phonons to the electronic structure, resulting in a modulation of the dielectric function. The slight frequency overestimation of this peak vs the experimental value of 1352 cm^{-1} (Table S1) is attributed to the known DFT overestimation for iTO phonons near the K-point.[36,37] The higher frequency peaks at ~1564 cm^{-1} and ~1568 cm^{-1} are associated with two phases of a C-C bond stretching mode polarized along the collapsed nanotube periodic axis. These resemble strongly the iTO graphene branch at the Γ-point, and are interpreted as the G

band. A smaller peak at 1603 cm^{-1} arises from a mode whose intensity modulates around the circumference of the collapsed nanotube. Its transversal displacements resemble the iLO graphene branch at the Γ-point, which coupled with its high frequency value allows attribution of this peak to the D' band of defective graphene (activated by cavities in the case of FCNTs).

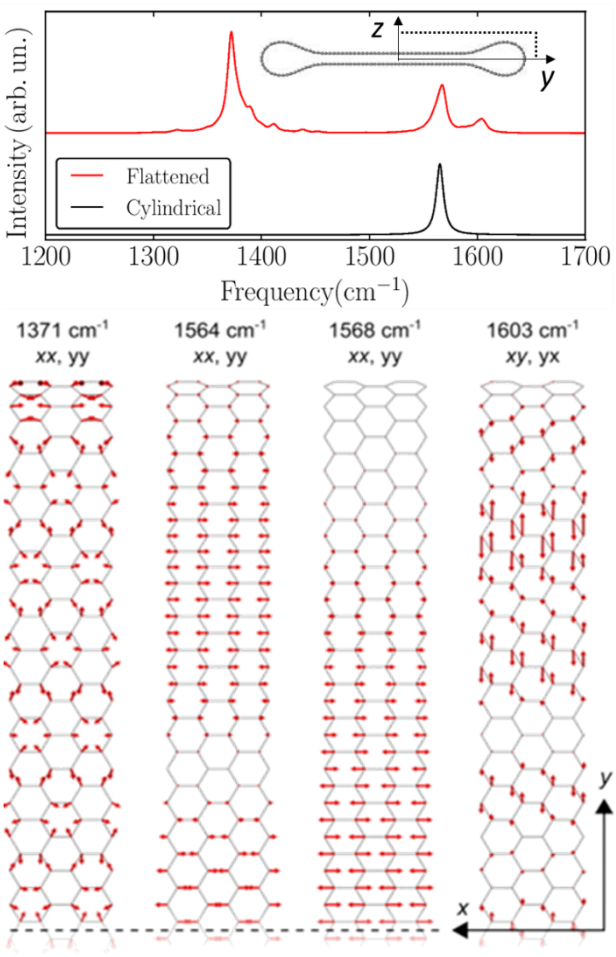

Figure 4 (Top) Calculated Raman spectrum of a zig-zag (70,0) carbon nanotube, either cylindrical or flattened with AB' stacking at 2.3 eV excitation energy (538 nm) (incident and scattered light polarization are averaged in the FCNT plane). (insert) cross-section of the structure for the flattened (70,0) (Below) Eigendisplacements of the strongest vibrations contributing to the Raman peak for the flattened (70,0). Each is labeled with its corresponding frequency and non-zero Raman tensor components in the flattened tube plane. Only the top-half and front-face of the tube is shown for clarity.

The Raman spectrum of a chiral FCNT (40,10) has also been computed (its width is smaller than the (70,0) to limit the number of atoms, since chiral tubes have longer unit cells along their axes). The same qualitative result was obtained, i.e. the appearance of a D band at 1352 cm^{-1} (2.5 eV excitation energy). As for the zig-zag FCNT, if restored to a circular cross-section the D band disappears. Furthermore, calculations for an armchair (50,50) nanotube at 2.3 eV excitation energy (538 nm) show an absence of peaks in the D band region, as expected on the basis of backscattering geometry by the wave vector of this specific edge[10] (vide supra) and as observed in the case of GNRs.

The interpretation of the D band origin for FCNTs presented here differs from that proposed in the literature for the same objects. Objects produced by sonication of arc-discharge MWCNTs in solution[22,23] were initially identified, instead of FCNTs, as GNRs that would have been produced via an unzipping process of the parent MWCNTs. The straight parallel lines showing dark contrast in HRTEM were proposed to be bending edges rather than FCNT lateral cavities. The small D/G intensity ratio (~0,5) first measured was used as an argument to prove the high quality of the GNR edges. Subsequent Raman characterisation of the objects showed a dependence of D band intensity with light polarization orientation relative to the object, with D/G intensity ratio sometimes up to almost 10.[23] This is consistent with our data but was attributed to D band behaviour of GNR edges instead of curvature. Tube extraction rather than unzipping, giving FCNTs instead of GNRs was later proposed and experimentally confirmed by Choi et al.[24] Our interpretation assigning the strong and sharp D band to FCNT cavities actually clear the apparent contradiction of a high D/G intensity ratio despite the good quality of objects and also matches the observation of a D band associated to a graphene fold by Gupta et al.[31]

CONCLUSIONS

The close correlation between Raman spectroscopy and AFM employed here serves to unambiguously identify Raman spectra of isolated flattened nanotubes. MWCNTs in the vicinity can be directly compared with the FCNTs. Knowing that the two families of objects have a comparable defect density confirms that the very intense and narrow D band observed in FCNT spectra does not come from structural defects but is, at least, activated by a line of curvature-induced hybridisation change along the two edge cavities. This activation is actually expected since this line behaves as a translational symmetry breaker between the flat and the cavity region. DFT calculations coupled with the Placzek approximation support this observation of a chemical defect free D band in FCNTs, reproducing the activation of phonon modes. This assignment is of great importance since D band intensity is commonly employed to quantify the amount of structural defects in carbon materials in general. We show here that in FCNTs, the D band is an inherent property of the FCNT geometry and not the consequence of a defective region. This folding-induced D band should be a general result, also valid for single folds in graphene[31] and buckling in annealed nuclear graphites,[38] reconstructed folded edges in carbon stacked platelet nanofibers,[39] platelet carbon nanofibers,[40] graphene nanoribbons,[41] hexagonal pyramidal hillocks,[42] cone-shaped graphenic whiskers,[43] graphenic polyhedral crystals[44,45] and elsewhere where symmetry in the carbon lattice is broken through a change in curvature. Reports describing graphenic materials where a D band is associated with poorly organised carbon or quantifying the amount of graphenic materials using I_D/I_G, might be revisited, particularly in cases of structural distortion such as those indicated above, induced by mechanical exfoliation, high-pressure measurements and high-temperature annealed materials. Finally, FCNTs represent a unique system to study the Raman of disorder activation without actual disorder being present.

METHODS

Experimental: After cap removal by thermal oxidation (580 °C, up to 72 % weight loss, 14475 Pa oxygen partial pressure), 5 mg of MWCNTs (Arc discharge synthesis, MerCorporation) have been tip sonicated for 1 hour in 15 ml of 1 %(w/v) aqueous solution of sodium cholate A drop of the diluted solution (1 to 4) have been deposited on a silicon surface coated with 300 nm silicon oxide. After rinsing with pure water, the surface was examined by AFM (Tapping mode, Bioscope Resolve Bruker), and a zone of interest was localized. Successive Raman mappings at selected wavelengths allows to find precisely the zone of interest and attribute a Raman spectrum to isolated objects. The perfect matching between the AFM height images and the Raman mapping is shown in ESI. For polarized measurements, the surface has been placed on a homemade turntable (see Fig. S6 ESI) and Raman mappings recorded every 10° rotation to unambiguously assign spectra to the objects, while the linear laser polarization was kept fixed. No analyzer was used. More precise experimental details are available in ESI.

Atomistic Simulations: All DFT computations are performed with the software package AIMPRO.[46,47] The exchange-correlation functional is treated by the generalized gradient approximation (GGA) parametrized by Perdew, Burke, and Ernzerholf (PBE) formalism.[48] Van der Waals are added by DFT-D2 scheme.[49] Hexagonal unit cells are used to contain circular nanotubes and orthorhombic cells for flattened carbon nanotubes, adopting periodic boundary conditions. A primitive cell is used for the zigzag case, the supercell is doubled along the periodic axis for the armchair tube. Both nanotube geometry and axial lattice vector were allowed to fully relax with no symmetry constraints. Reciprocal space is sampled by a 4×1×1 grid mesh using the Monkhorst-Pack formalism.[50] Cell sizes are large enough (e.g. at least 20 Å for nanotubes) to avoid interaction with periodic replicas.

The flattened zigzag (70,0) tube is 7.96 nm wide, the armchair (50,50) 10.21 nm. These are less than the experimental samples (~30 nm), but above the 7.65 nm width threshold where

collapse is thermodynamically favourable. Interlayer stacking in the central flattened section is set to the lowest energy cases imposed by the tube chirality, i.e. AB-stacking for the (50,50) armchair tube and AB'-stacking for the (70,0) zigzag tube.

Vibrational frequencies are determined by calculating energy and forces for ±0.106 Å atomic displacements. Phonon calculations use the second derivative of the energy with respect to atomic positions, using a finite difference scheme of the derivative from the calculated forces. The first derivative of the real and imaginary part of the dielectric function are calculated under the dipole approximation. Dielectric functions require an extremely high level of precision, and for this reason we used a dense 360x1x1 k-point grid with an electronic convergence criterion of 1×10^{-10} Ha. Raman intensity calculations are then performed within the Placzek approximation.[51,52] Full details are available in Supporting Information.

ASSOCIATED CONTENT

Supporting Information

Experimental details and computation, reference measurements, SEM images, Fit details, and polarized measurements.

AUTHOR INFORMATION

Corresponding Author

*E-mail: alain.penicaud@crpp.cnrs.fr

Author Contributions

EP performed most of the experiments with the help of FH, MB, JYM and HS. AI performed the DFT study helped by DR and CPE. LN, ACTD and MM contributed the microscopy images and analysis, EP, AI, DR, MB, JYM, FH, ACTD, JLD, MM, BH, PP, CPE and AP analysed the data and wrote the manuscript.

Notes

The authors declare no conflict of interest.

ACKNOWLEDGMENT

We thank the CNRS and Agence Nationale de la Recherche (ANR, project Edgefiller), Prof. Dr. S. Reich, M. Pimenta and E. Anglaret for stimulating discussions, P. Barboteau and E. Texier for the home-made Raman turn table and Dr. L. Buisson for technical help. AI, DR, and CPE acknowledge the CCIPL "Centre de Calcul Intensif Pays de la Loire" where many of the calculations were performed. FH thanks CNRS (Momentum project).

REFERENCES

(1) Saito, R.; Hofmann, M.; Dresselhaus, G.; Jorio, A.; Dresselhaus, M. S. Raman Spectroscopy of Graphene and Carbon Nanotubes. *Adv. Phys.* **2011**, *60* (3), 413–550. https://doi.org/10.1080/00018732.2011.582251.

(2) Ferrari, A. C.; Basko, D. M. Raman Spectroscopy as a Versatile Tool for Studying the Properties of Graphene. *Nat. Nanotechnol.* **2013**, *8* (4), 235–246. https://doi.org/10.1038/nnano.2013.46.

(3) Dresselhaus, M. S.; Dresselhaus, G.; Saito, R.; Jorio, A. Raman Spectroscopy of Carbon Nanotubes. *Physics Reports*. 2005, pp 47–99. https://doi.org/10.1016/j.physrep.2004.10.006.

(4) Verzhbitskiy, I. A.; De Corato, M.; Ruini, A.; Molinari, E.; Narita, A.; Hu, Y.; Schwab, M. G.; Bruna, M.; Yoon, D.; Milana, S.; Feng, X.; Müllen, K.; Ferrari, A. C.; Casiraghi, C.; Prezzi, D. Raman Fingerprints of Atomically Precise Graphene Nanoribbons. *Nano Lett.* **2016**, *16* (6), 3442–3447. https://doi.org/10.1021/acs.nanolett.5b04183.

(5) Saito, R.; Furukawa, M.; Dresselhaus, G.; Dresselhaus, M. S. Raman Spectra of Graphene Ribbons. *J. Phys. Condens. Matter* **2010**, *22* (33). https://doi.org/10.1088/0953-8984/22/33/334203.

(6) Kataura, H.; Kumazawa, Y.; Maniwa, Y.; Umezu, I.; Suzuki, S.; Ohtsuka, Y.; Achiba, Y. Optical Properties of Single-Wall Carbon Nanotubes. *Synth. Met.* **1999**, *103* (1–3), 2555–2558. https://doi.org/10.1016/S0379-6779(98)00278-1.

(7) Wu, J. Bin; Lin, M. L.; Cong, X.; Liu, H. N.; Tan, P. H. Raman Spectroscopy of Graphene-Based Materials and Its Applications in Related Devices. *Chem. Soc. Rev.* **2018**, *47* (5), 1822–1873. https://doi.org/10.1039/c6cs00915h.

(8) Puech; Kandara; Paredes; Moulin; Weiss-Hortala; Kundu; Ratel-Ramond; Plewa; Pellenq; Monthioux. Analyzing the Raman Spectra of Graphenic Carbon Materials from Kerogens to Nanotubes: What Type of Information Can Be Extracted from Defect Bands? *C — J. Carbon Res.* **2019**, *5* (4), 69. https://doi.org/10.3390/c5040069.

(9) Maultzsch, J.; Reich, S.; Thomsen, C. Double-Resonant Raman Scattering in Graphite: Interference Effects, Selection Rules, and Phonon Dispersion. *Phys. Rev. B* **2004**, *70* (15), 155403. https://doi.org/10.1103/PhysRevB.70.155403.

(10) Casiraghi, C.; Hartschuh, A.; Qian, H.; Piscanec, S.; Georgi, C.; Fasoli, A.; Novoselov, K. S.; Basko, D. M.; Ferrari, A. C. Raman Spectroscopy of Graphene Edges. *Nano Lett.* **2009**, *9* (4), 1433–1441. https://doi.org/10.1021/nl8032697.

(11) Cançado, L. G.; Pimenta, M. A.; Neves, B. R. A.; Dantas, M. S. S.; Jorio, A. Influence of the Atomic Structure on the Raman Spectra of Graphite Edges. *Phys. Rev. Lett.* **2004**, *93* (24), 247401. https://doi.org/10.1103/PhysRevLett.93.247401.

(12) Eliel, G. S. N.; Moutinho, M. V. O.; Gadelha, A. C.; Righi, A.; Campos, L. C.; Ribeiro,

H. B.; Chiu, P.-W.; Watanabe, K.; Taniguchi, T.; Puech, P.; Paillet, M.; Michel, T.; Venezuela, P.; Pimenta, M. A. Intralayer and Interlayer Electron–phonon Interactions in Twisted Graphene Heterostructures. *Nat. Commun.* **2018**, *9* (1), 1221. https://doi.org/10.1038/s41467-018-03479-3.

(13) Cançado, L. G.; Gomes da Silva, M.; Martins Ferreira, E. H.; Hof, F.; Kampioti, K.; Huang, K.; Pénicaud, A.; Alberto Achete, C.; Capaz, R. B.; Jorio, A. Disentangling Contributions of Point and Line Defects in the Raman Spectra of Graphene-Related Materials. *2D Mater.* **2017**, *4* (2), 25039. https://doi.org/10.1088/2053-1583/aa5e77.

(14) Eckmann, A.; Felten, A.; Mishchenko, A.; Britnell, L.; Krupke, R.; Novoselov, K. S.; Casiraghi, C. Probing the Nature of Defects in Graphene by Raman Spectroscopy. *Nano Lett.* **2012**, *12* (8), 3925–3930. https://doi.org/10.1021/nl300901a.

(15) Lucchese, M. M.; Stavale, F.; Ferreira, E. H. M.; Vilani, C.; Moutinho, M. V. O.; Capaz, R. B.; Achete, C. A.; Jorio, A. Quantifying Ion-Induced Defects and Raman Relaxation Length in Graphene. *Carbon N. Y.* **2010**, *48* (5), 1592–1597. https://doi.org/10.1016/j.carbon.2009.12.057.

(16) Chopra, N. G.; Benedict, L. X.; Crespi, V. H.; Cohen, M. L.; Louie, S. G.; Zettl, A. Fully Collapsed Carbon Nanotubes. *Nature* **1995**, *377* (6545), 135–138. https://doi.org/10.1038/377135a0.

(17) Liu, S.; Yue, J.; Wehmschulte, R. J. Large Thick Flattened Carbon Nanotubes. *Nano Lett.* **2002**, *2* (12), 1439–1442. https://doi.org/10.1021/nl0257869.

(18) Zhang, C.; Bets, K.; Lee, S. S.; Sun, Z.; Mirri, F.; Colvin, V. L.; Yakobson, B. I.; Tour, J. M.; Hauge, R. H. Closed-Edged Graphene Nanoribbons from Large-Diameter Collapsed Nanotubes. *ACS Nano* **2012**, *6* (7), 6023–6032.

https://doi.org/10.1021/nn301039v.

(19) Impellizzeri, A.; Briddon, P.; Ewels, C. P. Stacking- and Chirality-Dependent Collapse of Single-Walled Carbon Nanotubes: A Large-Scale Density-Functional Study. *Phys. Rev. B* **2019**, *100* (11), 115410. https://doi.org/10.1103/PhysRevB.100.115410.

(20) He, M.; Dong, J.; Wang, H.; Xue, H.; Wu, Q.; Xin, B.; Gao, W.; He, X.; Yu, J.; Sun, H.; Ding, F.; Zhang, J. Advance in Close-Edged Graphene Nanoribbon: Property Investigation and Structure Fabrication. *Small* **2019**, *15* (29), 1804473. https://doi.org/10.1002/smll.201804473.

(21) Terrones, M.; Botello-Méndez, A. R.; Campos-Delgado, J.; López-Urías, F.; Vega-Cantú, Y. I.; Rodríguez-Macías, F. J.; Elías, A. L.; Muñoz-Sandoval, E.; Cano-Márquez, A. G.; Charlier, J. C.; Terrones, H. Graphene and Graphite Nanoribbons: Morphology, Properties, Synthesis, Defects and Applications. *Nano Today* **2010**, *5* (4), 351–372. https://doi.org/10.1016/j.nantod.2010.06.010.

(22) Jiao, L.; Wang, X.; Diankov, G.; Wang, H.; Dai, H. Facile Synthesis of High-Quality Graphene Nanoribbons. *Nat. Nanotechnol.* **2010**, *5* (5), 321–325. https://doi.org/10.1038/nnano.2010.54.

(23) Xie, L.; Wang, H.; Jin, C.; Wang, X.; Jiao, L.; Suenaga, K.; Dai, H. Graphene Nanoribbons from Unzipped Carbon Nanotubes: Atomic Structures, Raman Spectroscopy, and Electrical Properties. *J. Am. Chem. Soc.* **2011**, *133* (27), 10394–10397. https://doi.org/10.1021/ja203860a.

(24) Choi, D. H.; Wang, Q.; Azuma, Y.; Majima, Y.; Warner, J. H.; Miyata, Y.; Shinohara, H.; Kitaura, R. Fabrication and Characterization of Fully Flattened Carbon Nanotubes: A New Graphene Nanoribbon Analogue. *Sci. Rep.* **2013**, *3* (1), 1617.

https://doi.org/10.1038/srep01617.

(25) Elliott, J. A.; Sandler, J. K. W.; Windle, A. H.; Young, R. J.; Shaffer, M. S. P. Collapse of Single-Wall Carbon Nanotubes Is Diameter Dependent. *Phys. Rev. Lett.* **2004**, *92* (9), 92–95. https://doi.org/10.1103/PhysRevLett.92.095501.

(26) He, M.; Dong, J.; Zhang, K.; Ding, F.; Jiang, H.; Loiseau, A.; Lehtonen, J.; Kauppinen, E. I. ESI for Precise Determination of the Threshold Diameter for a Single-Walled Carbon Nanotube to Collapse. *ACS Nano* **2014**, *8* (9), 9657–9663. https://doi.org/10.1021/nn5042812.

(27) Thomsen, C.; Reich, S. Double Resonant Raman Scattering in Graphite. *Phys. Rev. Lett.* **2000**, *85* (24), 5214–5217. https://doi.org/10.1103/PhysRevLett.85.5214.

(28) Yoon, D.; Moon, H.; Son, Y. W.; Samsonidze, G.; Park, B. H.; Kim, J. B.; Lee, Y. P.; Cheong, H. Strong Polarization Dependence of Double-Resonant Raman Intensities in Graphene. *Nano Lett.* **2008**, *8* (12), 4270–4274. https://doi.org/10.1021/nl8017498.

(29) Shinde, D. B.; Debgupta, J.; Kushwaha, A.; Aslam, M.; Pillai, V. K. Electrochemical Unzipping of Multi-Walled Carbon Nanotubes for Facile Synthesis of High-Quality Graphene Nanoribbons. *J. Am. Chem. Soc.* **2011**, *133* (12), 4168–4171. https://doi.org/10.1021/ja1101739.

(30) Brus, L. E.; Kim, P.; Ryu, S.; Han, M. Y.; Maultzsch, J. Raman Spectroscopy of Lithographically Patterned Graphene Nanoribbons. *ACS Nano* **2011**, *5* (5), 4123–4130. https://doi.org/10.1021/nn200799y.

(31) Gupta, A. K.; Nisoli, C.; Lammert, P. E.; Crespi, V. H.; Eklund, P. C. Curvature-Induced D-Band Raman Scattering in Folded Graphene. *J. Phys. Condens. Matter* **2010**, *22* (33), 334205. https://doi.org/10.1088/0953-8984/22/33/334205.

(32) Blase, X.; Benedict, L. X.; Shirley, E. L.; Louie, S. G. Hybridization Effects and Metallicity in Small Radius Carbon Nanotubes. *Phys. Rev. Lett.* **1994**, *72* (12), 1878–1881. https://doi.org/10.1103/PhysRevLett.72.1878.

(33) Kürti, J.; Zólyomi, V.; Grüneis, A.; Kuzmany, H. Double Resonant Raman Phenomena Enhanced by van Hove Singularities in Single-Wall Carbon Nanotubes. *Phys. Rev. B* **2002**, *65* (16), 165433. https://doi.org/10.1103/PhysRevB.65.165433.

(34) Borin Barin, G.; Fairbrother, A.; Rotach, L.; Bayle, M.; Paillet, M.; Liang, L.; Meunier, V.; Hauert, R.; Dumslaff, T.; Narita, A.; Müllen, K.; Sahabudeen, H.; Berger, R.; Feng, X.; Fasel, R.; Ruffieux, P. Surface-Synthesized Graphene Nanoribbons for Room Temperature Switching Devices: Substrate Transfer and Ex Situ Characterization. *ACS Appl. Nano Mater.* **2019**, *2* (4), 2184–2192. https://doi.org/10.1021/acsanm.9b00151.

(35) Rizzo, D.; Prezzi, D.; Ruini, A.; Nagyte, V.; Keerthi, A.; Narita, A.; Beser, U.; Xu, F.; Mai, Y.; Feng, X.; Müllen, K.; Molinari, E.; Casiraghi, C. Multiwavelength Raman Spectroscopy of Ultranarrow Nanoribbons Made by Solution-Mediated Bottom-up Approach. *Phys. Rev. B* **2019**, *100* (4), 45406. https://doi.org/10.1103/PhysRevB.100.045406.

(36) Jorio, A.; Cançado, L. G.; Malard, L. M. Vibrations in Graphene. In *2D Materials*; Avouris, P., Heinz, T. F., Low, T., Eds.; Cambridge University Press: Cambridge, 2017; pp 71–89. https://doi.org/10.1017/9781316681619.006.

(37) Reichardt, S.; Wirtz, L. Raman Spectroscopy of Graphene. In *Optical Properties of Graphene*; WORLD SCIENTIFIC, 2017; pp 85–132. https://doi.org/10.1142/9789813148758_0003.

(38) Heggie, M. I.; Suarez-Martinez, I.; Davidson, C.; Haffenden, G. Buckle, Ruck and

Tuck: A Proposed New Model for the Response of Graphite to Neutron Irradiation. *J. Nucl. Mater.* **2011**, *413* (3), 150–155. https://doi.org/10.1016/j.jnucmat.2011.04.015.

(39) Gan, L.; Du, H.; Li, B.; Kang, F. Surface-Reconstructed Graphite Nanofibers as a Support for Cathode Catalysts of Fuel Cells. *Chem. Commun.* **2011**, *47* (13), 3900. https://doi.org/10.1039/c1cc10179j.

(40) Yoon, S.-H.; Lim, S.; Hong, S.; Qiao, W.; Whitehurst, D. D.; Mochida, I.; An, B.; Yokogawa, K. A Conceptual Model for the Structure of Catalytically Grown Carbon Nano-Fibers. *Carbon N. Y.* **2005**, *43* (9), 1828–1838. https://doi.org/10.1016/j.carbon.2005.02.031.

(41) Campos-Delgado, J.; Kim, Y. A.; Hayashi, T.; Morelos-Gómez, A.; Hofmann, M.; Muramatsu, H.; Endo, M.; Terrones, H.; Shull, R. D.; Dresselhaus, M. S.; Terrones, M. Thermal Stability Studies of CVD-Grown Graphene Nanoribbons: Defect Annealing and Loop Formation. *Chem. Phys. Lett.* **2009**, *469* (1–3), 177–182. https://doi.org/10.1016/j.cplett.2008.12.082.

(42) Glad, X.; de Poucques, L.; Jaszczak, J. A.; Belmahi, M.; Ghanbaja, J.; Bougdira, J. Plasma Synthesis of Hexagonal-Pyramidal Graphite Hillocks. *Carbon N. Y.* **2014**, *76*, 330–340. https://doi.org/10.1016/j.carbon.2014.04.084.

(43) Saito, Y.; Arima, T. Features of Vapor-Grown Cone-Shaped Graphitic Whiskers Deposited in the Cavities of Wood Cells. *Carbon N. Y.* **2007**, *45* (2), 248–255. https://doi.org/10.1016/j.carbon.2006.10.002.

(44) Gogotsi, Y. Graphite Polyhedral Crystals. *Science (80-.).* **2000**, *290* (5490), 317–320. https://doi.org/10.1126/science.290.5490.317.

(45) Okuno, H.; Palnichenko, A.; Despres, J.-F.; Issi, J.-P.; Charlier, J.-C. Synthesis of

Graphite Polyhedral Crystals Using a Combustion Flame Method. *Carbon N. Y.* **2005**, *43* (4), 692–697. https://doi.org/10.1016/j.carbon.2004.10.033.

(46) Rayson, M. J.; Briddon, P. R. Rapid Iterative Method for Electronic-Structure Eigenproblems Using Localised Basis Functions. *Comput. Phys. Commun.* **2008**, *178* (2), 128–134. https://doi.org/10.1016/j.cpc.2007.08.007.

(47) Rayson, M. J.; Briddon, P. R. Highly Efficient Method for Kohn-Sham Density Functional Calculations of 500-10000 Atom Systems. *Phys. Rev. B* **2009**, *80* (20), 205104. https://doi.org/10.1103/PhysRevB.80.205104.

(48) Perdew, J. P.; Burke, K.; Ernzerhof, M. Generalized Gradient Approximation Made Simple. *Phys. Rev. Lett.* **1996**, *77* (18), 3865–3868. https://doi.org/10.1103/PhysRevLett.77.3865.

(49) Grimme, S. Semiempirical GGA-Type Density Functional Constructed with a Long-Range Dispersion Correction. *J. Comput. Chem.* **2006**, *27* (15), 1787–1799. https://doi.org/10.1002/jcc.20495.

(50) Monkhorst, H. J.; Pack, J. D. Special Points for Brillouin-Zone Integrations. *Phys. Rev. B* **1976**, *13* (12), 5188–5192. https://doi.org/10.1103/PhysRevB.13.5188.

(51) Talirz, L.; Söde, H.; Dumslaff, T.; Wang, S.; Sanchez-Valencia, J. R.; Liu, J.; Shinde, P.; Pignedoli, C. A.; Liang, L.; Meunier, V.; Plumb, N. C.; Shi, M.; Feng, X.; Narita, A.; Müllen, K.; Fasel, R.; Ruffieux, P. On-Surface Synthesis and Characterization of 9-Atom Wide Armchair Graphene Nanoribbons. *ACS Nano* **2017**, *11* (2), 1380–1388. https://doi.org/10.1021/acsnano.6b06405.

(52) Walter, M.; Moseler, M. Ab Initio Wavelength-Dependent Raman Spectra: Placzek Approximation and Beyond. *J. Chem. Theory Comput.* **2020**, *16* (1), 576–586.

https://doi.org/10.1021/acs.jctc.9b00584.